One-dimensional nanostructure-guided chain reactions: Harmonic and anharmonic interactions

Citation: Nair, Nitish , and Michael S. Strano. "One-dimensional nanostructure-guided chain reactions: Harmonic and anharmonic interactions." Physical Review B 80.17 (2009): 174301. © 2009 The American Physical Society

As Published: http://dx.doi.org/10.1103/PhysRevB.80.174301

Publisher: American Physical Society

Persistent URL: http://hdl.handle.net/1721.1/52449

Version: Final published version: final published article, as it appeared in a journal, conference proceedings, or other formally published context

One-dimensional nanostructure-guided chain reactions: Harmonic and anharmonic interactions

Nitish Nair and Michael S. Strano
Department of Chemical Engineering, Massachusetts Institute of Technology, Cambridge, Massachusetts 02139, USA
(Received 26 April 2009; revised manuscript received 18 August 2009; published 13 November 2009)

We have performed a parametric study of self-propagating chain reactions along a one-dimensional bead-spring array. The coupling between beads is modeled using harmonic and anharmonic Fermi-Pasta-Ulam (FPU)-β and φ^4 potentials. The parameters that define the system are the activation energy (E_a) of the reactive group and the fraction (α) of the reaction enthalpy that is converted to the kinetic energies of the reacted products. The mean conversion for a 100-bead lattice was investigated as a function of these handles. Assemblies of pristine chains with reactive groups having $E_a < 25$ kcal/mol are shown to be inherently unstable. At loads of 3–4 energetic molecules/bead ($E_a = 35$ kcal/mol, $\alpha = 0.7$), the FPU and harmonic lattices behaved similarly with reaction velocities ranging between 8 and 8.5 km/sec. The φ^4 lattice exhibited lower conversions along with the formation of a reaction initiation zone where the velocity was at least half of the bulk value at the aforementioned loads. Fourier analyses of the kinetic energy traces of the φ^4 lattice revealed that only high-frequency excitations led to viable wave propagation, which explains the prominence of the start-up zone at lower loadings of the energetic molecules. High velocity reaction waves are only observed in perfect crystal arrays. The presence of defects in the chain, i.e., beads with weaker force constants, hampers the progress of the wave.

DOI: 10.1103/PhysRevB.80.174301 PACS number(s): 66.70.−f, 63.20.Ry, 63.22.Gh

I. INTRODUCTION

One-dimensional (1D) chains with different potential functions have been extensively studied with respect to their dynamical properties,[1] shock waves,[2–4] bond dissociation,[5] energy relaxation,[6,7] and pulse propagation.[8,9] We use this simple platform to model sustained chain reactions that propagate in a single dimension, as along the backbone of a carbon nanotube. Single-walled carbon nanotubes (SWNT) are cylindrical graphene sheets[10,11] that have high thermal conductivities, as shown by considerable theoretical[12–16] and experimental[17,18] efforts. Energetic groups bonded to the lattice react such that the energy released is coupled back into the nanostructure and directed along the backbone to propagate the reaction. The hypothesis is that the reduced dimensionality of the nanostructure should be able to guide and accelerate the reactions along a preferred orientation. Apart from their utility as thermal interface materials,[19,20] the quasi-one-dimensional nature of SWNT also holds prospects for applications as waveguides based on past work on confined propagation of x-rays[21] and thermal neutrons[22] through them.

Force fields allowing n-dimensional ($n \geq 1$) motion of the beads in a chain have been developed for fracture studies,[23,24] elastic deformations and self-assembly phenomena,[25] and simulations of the nanomechanics of single-walled carbon nanotubes.[26] Coarse-graining a complex three-dimensional (3D) molecule deprives it of most of its vibrational modes; however, it leads to a significant reduction in computation time in order to easily access picosecond time scales. The Zhigilei model[26] includes a potential corresponding to breathing modes that describes the internal degrees of freedom of the structure.[27–29] Their effect, along with that of torsion, were seen to be minimal in the case of isolated nanotubes.[26] In this work, we have used the Buehler model[25] as a simple representation of a carbon nanotube. The bond-stretch component of the total potential energy uses a bilinear expression derived from a harmonic potential, which accounts for nonlinearities up to a limit. Anharmonic potentials have been shown to produce solitons[30,31] and breathers[32] in crystal lattices. The mobility of high-energy fluctuations in a one-dimensional lattice depends on the type of nonlinearity present in the force field. The fluctuations may result in localized high-frequency oscillations in a lattice with an onsite potential characterized by the hard φ^4 term,[33] which leads to the so-called "diagonal anharmonicity"[34]—the interactions between neighboring beads is purely harmonic, while the anharmonicities are inherent within each oscillator, as represented by the onsite potential. Confined high-frequency oscillations—"breathers"—adversely affect the thermal conduction properties of the crystal due to the localization of energy.[33,35] The mobility of such oscillations is greatly enhanced through the use of an "off-diagonal" nonlinearity[36] such as the classic Fermi-Pasta-Ulam β (FPU-β) lattice.[1] In this case, the anharmonicity is embedded in the interbead interactions. From a mathematical standpoint, a "diagonal" or off-diagonal anharmonicity depends on the positions of nonlinear terms in the force-constant matrix of the system of oscillators.

We seek to harness the one-dimensionality and thermal conductivity of SWNT in modeling and simulating chain reactions of energetic molecules (EM) that have been covalently attached to the nanotube sidewall. A continuum model that describes the use of SWNT as thermal conduits has been framed,[37] but here we aim to track the directed thermal transfer process at the molecular scale. There is a wealth of experimental data on the reactions of metallic and semiconducting nanotubes with diazonium salts bearing OH, Cl, and NO_2 functional groups.[38–41] The same techniques can be used to functionalize SWNT with reactive molecules whose thermal decomposition reactions are highly exothermic. Molecular analogs of trinitrotoluene (TNT) and cyclotrimethylenetrinitramine (RDX) may be covalently bonded to the nanotube surface for this purpose. We have experimentally explored laser-ignited reactions and the concomitant thermopower generation in RDX-coated carbon nanotube ar-

rays. The superior thermal conduction of the nanotube backbone leads to a higher reaction velocity as compared to a pure RDX crystal. This amplified anisotropic velocity could aid in the creation of nanothrusters that exceed the specific impulse of any system demonstrated to date. An electrical wave is generated in the same direction as the thermal wave, which could supply nanoscale electronic devices with extremely high power densities. The current theoretical study is confined to the thermal propagation brought about by highly exothermic chain reactions in a coarse-grained lattice.

Each bead in the lattice is loaded with energetic molecules at a specified density. An excitation applied at one end of the chain is expected to raise the local temperature at the reaction sites leading to the decomposition of the group. The one-dimensionality can be used to channel the energy released during combustion and facilitate subsequent reactions. We seek to identify conditions under which sustained chain reactions are feasible. The following system parameters are varied: (a) activation energy of the reaction, E_a; (b) fraction of the reaction enthalpy that is converted into the kinetic energy (KE) of the reacted fragments, α. In the simulations, we have allowed α to vary from 0 to 1. Zones of chemical stability of the nanostructure as well as the velocity of the reaction wave have been mapped out. A Fourier analysis of the time-series of the kinetic energy of the lattice was performed to determine the modes that were responsible for the propagation of a disturbance through the lattice. The effect of loading of the EM has also been studied for pristine and defect-laden chains.

We emphasize that although the bead-spring array uses parameters for a specific force field in the literature,[25] our conclusions are not limited by this. In nondimensionalizing the equations of motion, the force constants have been scaled with respect to the tensile spring constant, which makes the model and the analysis generic. We have also introduced additional terms to account for anharmonicities for comparison, and this allows one to study their implications for nonlinear dynamics. The results presented in this paper are applicable to a broad class of idealized, one-dimensional oscillators. We refer to the force field describing the mechanics of carbon nanotubes only as a way to motivate experimental realization. We are aware that a quantitative comparison between the 1D array and the complex 3D molecular structure of a nanotube is impossible. Therefore, we try to establish a qualitative bridge between these two cases, set design criteria, and predict what may be observed when future experiments are performed in the laboratory.

II. MODEL DEVELOPMENT

A. Types of Lattices

The Hamiltonian (H) for a system of N oscillators as a function of the individual momenta (p_i), masses (m_i) and position vectors ($\vec{r}_i$) is

$$H = \sum_{i=1}^{N} \frac{p_i^2}{2m_i} + \frac{1}{2}[V(|\vec{r}_{i+1} - \vec{r}_i| - r_0) + V(|\vec{r}_i - \vec{r}_{i-1}| - r_0)] + U(|\vec{r}_i - \vec{r}_{i0}|), \quad (1a)$$

where $V(\gamma_{ij})$ is the interaction potential, and γ_{ij} is the deviation of the i-j bond length from its equilibrium value, r_0 (10 Å); $U(\delta_i)$ is the onsite potential, with δ_i denoting the displacement of the i^{th} oscillator from its equilibrium position, r_{i0}. The analytical forms of $V(\gamma_{ij})$ and $U(\delta_i)$ change according to the type of lattice used. The nondimensionalization of Eq. (1a) yields a time scale [t_{sc}, Eq. (1b)] that depends on the tensile force constant (k_s=1000 kcal/mol/Å^2) and the total mass in terms of the mass of a bead (m_b =1953 amu), the mass of the reactive group (m_e) and the total number of energetic groups loaded on each bead (n_0). The value of m_e depends on the reactive molecule chosen. For a given energy input, larger values of m_b or r_0 would adversely affect thermal propagation through the lattice due to the following reasons, respectively: (i) increased inertia of each bead; (ii) greater distance required for energy transfer to take place between neighboring beads.

$$t_{sc} = \sqrt{\frac{m_b + n_0 m_e}{k_s}}. \quad (1b)$$

The details of the harmonic potential in Eq. (2) along with the associated parameters have already been outlined in previous papers by Buehler and co-workers.[23–25]

$$V(\gamma_{ij}) = \frac{k_s}{2}\gamma_{ij}^2. \quad (2)$$

In the following expressions for anharmonic lattices, the emphasis will be on the tensile component of the force field, since the bond-angle and Lennard-Jones contributions will remain unchanged. The FPU-β lattice has a quartic term in addition to the harmonic portion and no onsite potential, $U(\delta_i)$.

$$V_{ij}(\gamma_{ij}) = \frac{k_s}{2}\gamma_{ij}^2 + \frac{k_s'}{4}\gamma_{ij}^4. \quad (3)$$

The nonlinear term plays a greater role at higher deformations. The frequency of oscillation increases with the energy input into the lattice, which results in a pulse propagating at a higher speed and lower dispersion than in a harmonic chain.[8,9]

The φ^4 lattice retains the pure harmonic interactions between beads but includes an external contribution in the form of a nonzero onsite potential

$$U(\delta_i) = \frac{k''}{2}\delta_i^2 + \frac{k'''}{2}\delta_i^4, \quad (4)$$

which represents the effect of a substrate or the environment of the chain on the motion of the i^{th} bead. The nonlinearity is embedded within the oscillator itself, thus resulting in diagonal anharmonicity. We have kept the same force constants for the harmonic and nonlinear components of the interaction potentials, i.e., $k_s'=k_s$ and $k''=k'''=k_s$ for the FPU-β and φ^4 chains, respectively.

B. Reaction Times

Reactions at the molecular scale are stochastic in nature because of fluctuations in temperature and pressure. In order

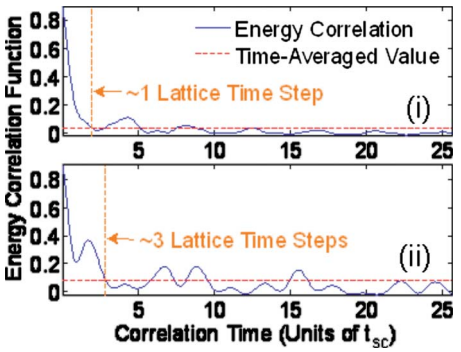

FIG. 1. (Color online) Estimation of the reaction acceptance criterion for the (i) FPU and (ii) φ^4 lattices: The excited bead relaxes after 1 (3) oscillation period of the lattice for the FPU (φ^4) case; the reaction is accepted if the computed time required for it is less than t_{sc} ($3t_{sc}$).

to predict the time at which one will occur and its position in the chain of oscillators, we use Gillespie's First-Reaction Method.[42] With the help of the Arrhenius formula, zeroth-order rates for each bead (k_i) are calculated in terms of the activation energy (E_a) and the kinetic energy of the bead in question ($E_{k,i}$)

$$k_i(s^{-1}) = 10^{13} \exp\left(-\frac{E_a}{E_{k,i}}\right). \tag{5}$$

The time at which a reaction will occur at the i^{th} bead is obtained by sampling the governing probability distribution for a zero-th order reaction[42]

$$P_i(\tau)d\tau = k_i \exp(-k_i\tau)d\tau. \tag{6}$$

The reaction times (τ) calculated are sorted in ascending order and the bead with the smallest time is chosen. The reaction location, μ, and time, τ_μ, can therefore be estimated together. The Gillespie algorithm simulates a Markovian process so only one reaction event is permitted within the time step considered.[42] If the activation energy is high enough, the reaction will be a localized event. The smallest value of τ at a particular node implies that the latter is energetic enough to satisfy the acceptance criterion for the reaction, which has been detailed in the subsequent section.

C. Reaction Acceptance Criterion

We use the Gillespie algorithm[42,43] to simultaneously predict the reaction location, μ, and time, τ_μ. Once a possible reaction site has been located by this technique, it remains to be seen whether it can be accepted or not. The metric we use compares the computed reaction occurrence time (τ_μ) with the time scale of energy dissipation in a quiescent lattice. A reaction may be accepted if a bead remains in an excited state for a sufficiently long period. To estimate the dissipation time scale, a bead in the center of the chain was excited and its KE was tracked as a function of time. The energy correlation function was computed from this time series for the FPU-β and the φ^4 lattices (Fig. 1). Panel (i) shows that relaxation occurs within one oscillation period (i.e., t_{sc}) for the FPU lattice, which is the norm for harmonic chains.[34] Anharmonicities in the potential function cause the dissipation to occur over longer time scales,[33] which is obvious for the φ^4 lattice in panel (ii), where at least three lattice time steps are required to achieve dissipation. Using the information in Fig. 1, we can execute a reaction if $\tau_\mu < t_{sc}$ (FPU-β) or $\tau_\mu < 3t_{sc}$ (φ^4). Despite the greater leeway given to the φ^4 lattice as compared to the FPU-β, we shall see that it has a lower reactivity than the latter for the same energetic load.

When multiple energetic molecules are loaded on a single bead, the coarse-grained nature of the system prevents us from ascertaining the time at which each group will react. In other words, the computed reaction time—τ_μ—applies to the entire node-reactive group assembly. We introduce stochasticity by permitting n_r energetic molecules on a bead to react if $n_r\tau_\mu < mt_{sc}$, where $m=1$ or 3 depending on the lattice considered. It is important to note that the dissipation time is a lower bound because it has been estimated for a quiescent lattice, i.e., one in which no reactions are taking place after the initial excitation. When prior reactions have occurred, an energetic bead will take longer to relax due to energy transfer from its predecessors.

D. Energy Conversion

The total energy (TE) of the entire lattice before a reaction event at a bead j depends on: (a) E_p—the potential (PE)—and E_k—the kinetic (KE)—energies of the lattice; (b) N, the number of beads; (c) n_0, the EM loading on each bead; (d) ΔH (<0), the enthalpy of reaction of a single EM

$$TE = E_p + E_k - N(n_0\Delta H). \tag{7a}$$

The last term gives the total energy stored in the EM-bead bonds. After n_r ($\leq n_0$) reactions have taken place at j, TE may be rewritten in terms of the new PE (E_p') and KE (E_k') of the lattice and the heat lost to the surroundings (Q)

$$TE = E_p' + E_k' - (Nn_0 - n_r)\Delta H + Q. \tag{7b}$$

The part of the reaction enthalpy that has not been lost partitions into the PE and KE of the affected bead. We shall now probe each term in the above equations for greater clarity:

(a) The lattice PE is assumed to remain invariant because the change in conformation due to the reaction is highly localized. This is plausible when the number of beads is large.

(b) The lattice KE prior to the reaction is given by $E_k = \frac{1}{2}\Sigma_{i=1}^{N}(m_b + n_0m_e)u_i^2$. After n_r reactions have occurred at bead j, it is modified to

$$E_k' = \left[\frac{1}{2}\sum_{i\neq j}(m_b + n_0m_e)u_i^2\right] + \left[\frac{1}{2}(m_b'v_{b,j}^2 + n_rm_ev_e^2)\right]. \tag{7c}$$

The first sum extends over the unreacted beads with the assumption that their velocities are not altered by the reaction. The second term is a sum of the KE of the reaction fragments: (a) the bead to which n_0-n_r EM are still attached, with a mass given by $m_b' = m_b + (n_0 - n_r)m_e$; (b) the center of mass of the decomposition products of the n_r energetic molecules. The latter are not tracked individually, since we are con-

cerned only with the effect of the reaction enthalpy on the lattice.

(c) The amount of energy lost irreversibly to the surroundings as heat is parameterized as a fraction of the reaction enthalpy. If a portion, α, of the energy released—$n_r\Delta H$—is converted to useful work, then $Q=(1-\alpha)n_r\Delta H$.

Equating the total energy before and after the reaction and substituting the expressions above, we get

$$2\alpha n_r\Delta H = m_b' v_b^2 + n_r m_e v_e^2 - (m_b + n_0 m_e)u^2. \tag{7d}$$

The velocities in Eq. (7d) can be expanded in terms of their (x,y,z) components

$$2\alpha n_r\Delta H = \sum_{j=x,y,z} [m_b' v_{b,j}^2 + n_r m_e v_{e,j}^2 - (m_b + n_0 m_e)u_j^2] = \sum_{j=x,y,z} E_{k,j}, \tag{7e}$$

where the right-hand side is the total KE across the spatial dimensions. If β_j is the fraction of ΔH available to dimension j, the left-hand side may be partitioned into 3 components, ε_j, such that $\varepsilon_j=\beta_j(2\alpha n_r\Delta H)$. The total energy balance can be split into dimensionwise portions with the appropriate velocity components.

$$\varepsilon_j = m_b' v_{b,j}^2 + n_r m_e v_{e,j}^2 - (m_b + n_0 m_e)u_j^2. \tag{7f}$$

In a given time step, only the final velocities—$v_{b,j}$ and $v_{e,j}$—are unknown. The simultaneous solution of Eq. (7f) with the conservation of momentum in each spatial dimension,

$$(m_b + n_0 m_e)u_j = m_b' v_{b,j} + n_r m_e v_{e,j}, \tag{7g}$$

yields them exactly

$$v_{b,j} = u_j \pm \sqrt{\frac{\varepsilon_j/(n_r m_e)}{\eta(\eta-1)}}, \tag{7h}$$

where $\eta=\frac{m_b}{n_r m_e}+\frac{n_0}{n_r}$. The choice of the sign is governed by momentum conservation.

E. Evaluation of β

The parameter β_j can be derived by assuming that the direction cosines, $\cos\theta_j=\frac{u_j}{|\vec{u}|}$, remain invariant immediately before and after the reaction. Here, θ_j is the angle made by the velocity vector, $\vec{u}$, with the j axis, where j stands for either x, y, or z. We suppose that during an infinitesimal time interval after the reaction, the center of mass of the decomposed EM moves along the same trajectory as the unreacted bead prior to the reaction. It is evident from Eq. (7h) that the final velocity components of the reacted bead are functions of ε_j, which itself depends on β_j. Using the invariance of the direction cosines and the fact that $v_{b,j}\sim\sqrt{\beta_j}$, β_j is found to be

$$\beta_j = \cos^2\theta_j \quad [j=x,y,z]. \tag{8}$$

Equation (8) has the following implication: if, for instance, the angle made by the trajectory of the unreacted bead with the x axis is smaller than those made with the other axes, there is a greater likelihood of the energy released augmenting the x component of the reacted bead's velocity.

III. RESULTS AND DISCUSSION

A. Parametric Study of Reactions

The number of beads in the chain (N) was fixed at 100. We performed the analysis for loads of one to seven reactive groups/bead. The energetic moiety used in the simulation is trinitrobenzene diazonium with a molecular mass (m_e) of 212 amu. In this section, we have presented results for the 3–4 EM/bead cases while those for the remaining loads have been included in the supplement.[44] The heat of decomposition of TNT (2732.48 kJ/kg)[45] was used as a representative value for ΔH.

The first step was to ascertain the stability—a measure of inertness of the lattice in the absence of ignition at 300 K—of the nanomaterial as a function of E_a and α. After equilibration, the system was allowed to evolve for ~7 ps and reaction events were recorded. The average chemical conversion is the ratio of the mean number of reaction events over 100 independent trials to the number of beads in the lattice. These conversions have been plotted in Figs. 2(a)–2(d) for different loads as a function of the 2 parameters. There exists a threshold of stability with spontaneous reactions occurring when $E_a<25$ kcal/mol. Approximately 80% of the reactive groups react without an external stimulus for $E_a<20$ kcal/mol; the obvious conclusion is that at low activation barriers, the reaction sites are energetic enough to obviate the need for a prior excitation. Most of the species react haphazardly at room temperature thereby making the assembly inherently unstable. This test establishes a lower limit for the selection of molecules in the design of such structures.

The effect of an excitation at $t=0$ was studied by permitting all the reactive groups at the first bead to react unconditionally and tracking the progress of the reaction wave with time. Figure 3 shows the total conversion as a function of the system parameters for (a)–(c) harmonic, FPU and φ^4 lattices at 3 reactive groups/bead, and (d)–(f) the respective lattices at four reactive groups/bead. As the reactive group load increases, a steep drop is observed between regions of almost complete and no conversion. An upper bound on α is necessary according to the second law of thermodynamics but this has not been implemented in the current work. The randomization of energy into other vibrational modes and its dissipation to the surroundings are reflected in lower values of α. The latter phenomenon can be minimized by utilizing an array of nanotubes such that the energy lost by one tube may be captured by another thus maintaining a high effective α for the entire structure.

While the conversion plots for the harmonic and FPU systems are almost identical for the loads used, the φ^4 lattice exhibits a lower conversion at each value of α. This can be attributed to the poor thermal conduction characteristics of the hard φ^4 potential.[33] Nonlinear 1D lattices can support a temperature gradient, as has been proved by nonequilibrium molecular dynamics simulations.[35,44,47] The approximate thermal conductivity of each chain can be found by calculating the ratio of the time-averaged heat current to the applied

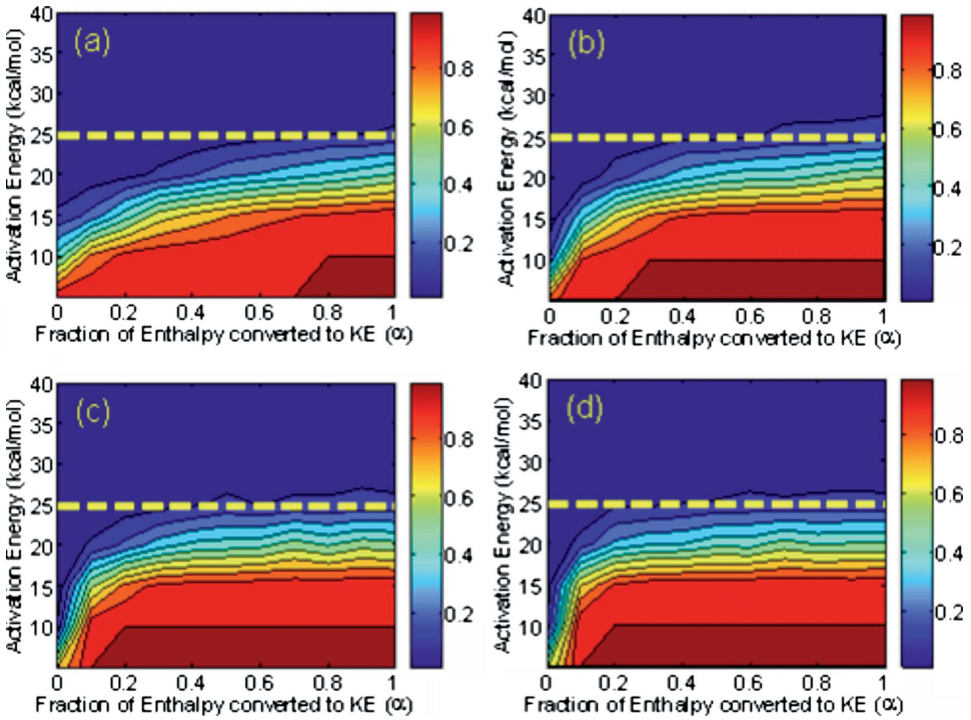

FIG. 2. (Color online) Stability plots in terms of chemical conversion without initial excitation for three loadings: (a) 1 EM/bead, (b) 2 EM/bead, (c) 3 EM/bead, and (d) 4 EM/bead. The nanostructures are unstable for E_a <25 kcal/mol (dotted line).

temperature gradient.[47–50] The thermal conductivity of the φ^4 lattice in our study is lower than that of the FPU chain by a factor of ~ 14.[44]

The difference between the harmonic and FPU lattices is minimal due to the small displacements of the beads from their equilibrium positions. As a result, the quartic term does not play a significant role under the current energetic loadings. The use of a considerably higher reaction enthalpy will be explored later to elicit the difference in the speed of wave propagation in these two lattices. For loads of one reactive group/bead or less (data not shown), negligible differences are observed between cases of finite and zero initial excitation. This is understandable, since the sparse coverage of en-ergetic molecules leads to minimal momentum exchange with the bead in the event a reaction occurs. The probability of a sustained reaction wave is therefore small; however, if E_a is low enough, reactions will take place haphazardly along the length of the chain. A minimum load of 3 EM/bead—alternatively, one group/54 C atoms on the nanotube basis—is required in order to generate a sustainable wave for the ΔH under consideration. This load can be achieved experimentally, since extents of reaction of at least 1 diazonium

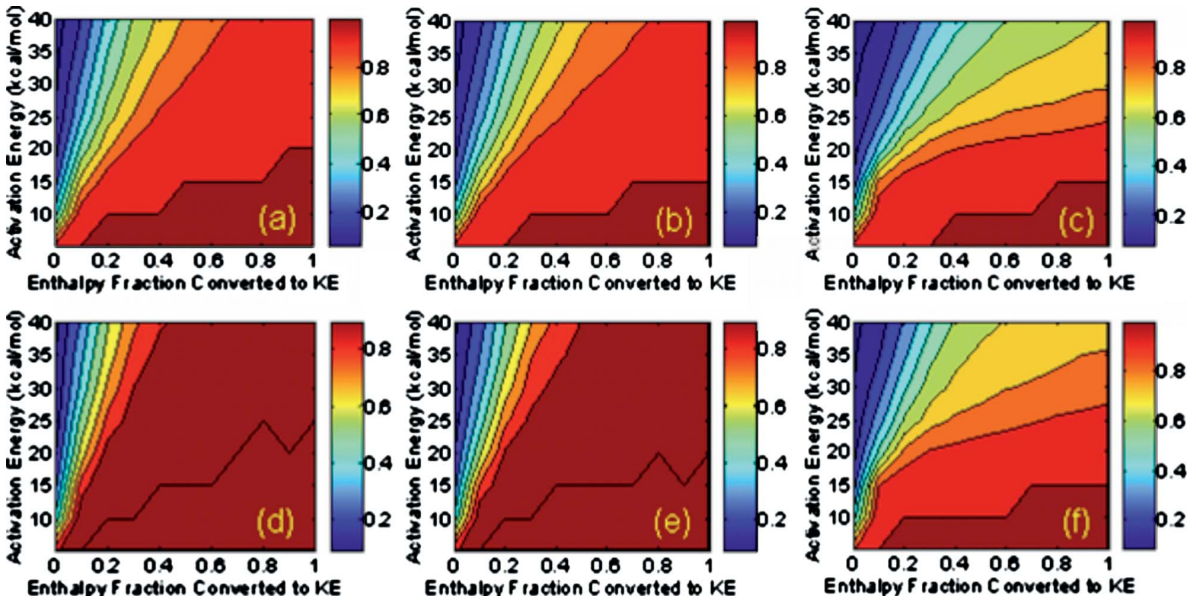

FIG. 3. (Color online) Chemical conversion plots for (a) harmonic, (b) FPU, and (c) φ^4 lattices at 3 EM/bead; (d)–(f) conversion plots for the respective cases at 4 EM/bead after equilibration at 300 K and allowing the first bead to react.

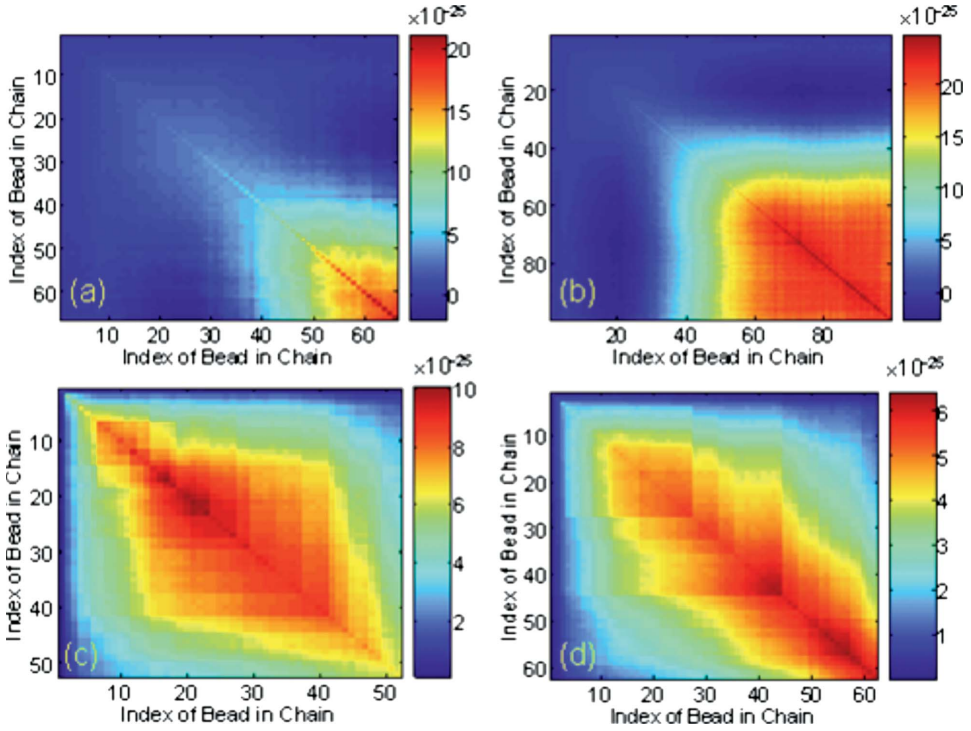

FIG. 4. (Color online) Covariance of the computed reaction times in units of sec^2 for the (a) and (b) harmonic, and (c) and (d) φ^4 lattices with loads of (a), (c) 3 EM/bead, and (b), (d) 4 EM/bead (E_a=35 kcal/mol, α=0.7).

group per 20 carbon atoms have been observed previously.[41]

The reaction time (τ) estimated by the Gillespie algorithm is a random variable. Each panel in Fig. 4 shows the covariance of these computed times, i.e., the effect of a reaction event at node i on sites further along the chain as a function of loading and the post-reaction energy available to the lattice. The steadily increasing pixel intensities down the length of the chain—along the main diagonal—indicate progressively greater correlations between neighboring reactive sites. For the harmonic lattice at loads of three and four reactive groups/bead, we see in Figs. 4(a) and 4(b), respectively, that the variance in reaction times increases with loading. The increased energy content of the lattice causes the beads near the point of ignition to react within a constrained set of times. With each successive reaction at subsequent beads, more energy is deposited into the lattice accompanied by the dispersion of the energetic pulse as it traverses the harmonic chain.[8,9] Consequently, the reaction front continuously broadens and subjects the beads ahead to constant excitation, thus enabling them to react before the front has passed them by. Identical reaction conditions for the φ^4 lattice present a contrary set of results [Figs. 4(c) and 4(d)] wherein the variance in reaction times decreases with increasing loads and is also lower than the corresponding values for the harmonic system. This shows that a greater degree of control over the progression of the reaction wave is afforded by the nonlinear φ^4 potential as compared to the harmonic.

In order to explain the above phenomenon, we examined the change in the phonon density of states (DOS) of the φ^4 lattice with reactions at loads of 3–7 and 12 reactive groups/bead.[44] A band gap partitions the spectrum into low- and high-frequency regions. The ratio of the area under the high-frequency portion to the total spectral area was recorded as a function of loading of the energetic molecules. The total contribution of the higher modes is directly proportional to the reactive group loading.[44] In the next subsection, we shall demonstrate that only signals with frequencies lying in the higher end of the spectrum have a finite probability of traveling through the φ^4 lattice. Therefore, energetic reactions with a sparse coverage of reactive groups excite the low-frequency modes to a greater extent, which have a limited capacity to propagate in the φ^4 chain. This decreases the efficiency of information transfer in the lattice and consequently raises the uncertainty in reaction times.

B. Fourier Analysis

The phonon density of states is generally measured by taking the Fourier transform of the velocity autocorrelation function.[51,52] The spectral analysis of the time-trace of the kinetic energy of the lattice can also be used[20,53] as a method to estimate the DOS. The frequencies (ω) have been expressed as multiples of the frequency of a lattice devoid of energetic molecules ($\omega_0=\sqrt{\frac{k_s}{m_b}}$). In order to understand why the conversion in the φ^4 lattice is less than the FPU and harmonic cases, it is important to analyze the DOS of each lattice as shown in Fig. 5(a). Additionally, we have mapped out the range of frequencies that support signal transduction in each lattice for a load of three reactive groups/bead. This range was determined by a technique similar to that used by Bowman *et al.* to obtain normal modes without a Hessian using Driven Molecular Dynamics.[54] The 50th bead in the chain was driven at various frequencies and the total kinetic energy of 40 beads on either side of the point of application of the signal was recorded. It is clear that viable propagation is possible at all the permitted frequencies ($0 \leq \omega \leq 0.6$) for the FPU and harmonic chains; however, only high-frequency signals ($0.3 \leq \omega \leq 0.65$) have nonzero probabilities of traveling through the φ^4 lattice. The effects of specific driving

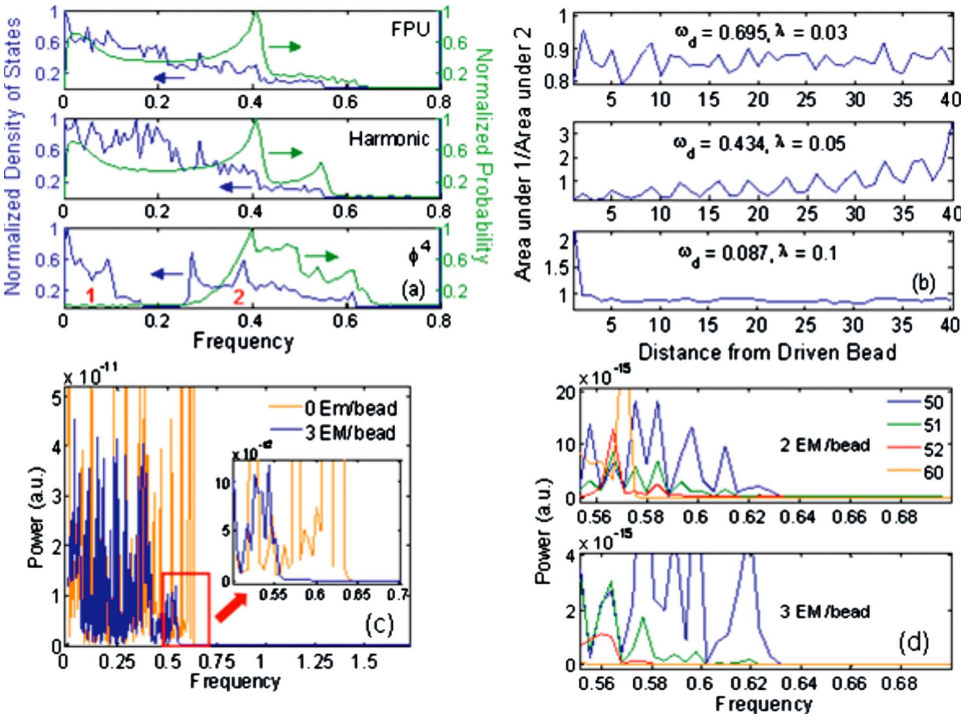

FIG. 5. (Color online) (a) Superposition of the DOS for the three lattices and the signal transmission probability. (b) Ratio of the contribution of lower modes [area 1 in Fig. 5(a)] to their higher counterparts [area 2 in Fig. 5(a)] at different driving frequencies (ω_d) and their respective optimal amplitudes (λ). (c) Fourier analysis of kinetic energy time series for the harmonic chain at 0 and 3 EM/bead. (d) Power spectra of four individual harmonic beads in the high-frequency range showing the induction of modes in the heavier beads (51, 52, 60) by the lighter one (50).

frequencies (ω_d) are depicted in Fig. 5(b) for the φ^4 chain. Each frequency, ω_d, has an optimal amplitude, λ,[44,54] whose value is also shown in each panel. The ratio of the areas under the regions labeled "1" and "2" in the bottom panel of Fig. 5(a) has been plotted against the distance from the 50th bead in Fig. 5(b). This ratio is a measure of the relative contributions of the low- and high-frequency modes to signal propagation. The top and bottom panels in Fig. 5(b) show a value close to 1 for the ratio, which remains almost constant with distance from the driven bead, thus implying that no energy transfer occurs between the higher and the lower modes. This is not surprising, since the corresponding ω_d lie in the forbidden range (i.e., $\omega_d < 0.3$ and $\omega_d > 0.65$). The central panel uses a driving frequency that lies in the permitted range; despite the noise, a distinct increase is observed in the ratio with distance, indicating that the role of the lower modes gradually grows in importance as one moves away from the driven bead. A transfer of energy takes place from the higher modes to the lower modes. In other words, the allowed high-frequency phonons from the point of excitation disintegrate into their low-frequency counterparts, which are responsible for the successful propagation of the wave. When compared to the FPU and harmonic lattices where all frequencies are allowed, only the upper half of the spectral range in the φ^4 chain is capable of transmitting signals. Oscillations with $\omega > 0.65$ become highly localized and possibly lead to the formation of breathers. This reduced capacity of the φ^4 chain to support signals of all permitted frequencies explains the poor conduction, and hence, lower chemical conversion when compared to the other two systems.

It is also of interest to determine whether a sustained reaction wave is facilitated by the activation of certain modes of oscillation in the harmonic lattice. Figure 5(c) shows the power spectra for zero and three reactive groups/bead calculated at 300 K. The absence of modes in the frequency range $0.55 < \omega < 0.66$ for the loaded chain (inset) is due to the fact that its component beads are heavier than the unloaded case, and the oscillation frequency is inversely proportional to mass. A lattice undergoing chain reactions will have a mix of completely reacted (i.e., lighter) and unreacted (i.e., heavier) beads. The above frequency range will play an important role in these circumstances especially since a rise in temperature increases the phonon population at the band-edge. Additionally, we see in the central panel of Fig. 5(a) that signals with frequencies $\omega \leq 0.4$ have a greater likelihood of penetrating a lattice loaded with three reactive groups/bead. It is evident that energy propagation in the lattice is carried out by the low-frequency portion of the spectrum. Modes above $\omega = 0.57$ do not contribute to propagation at all but we will show that they are capable of inducing reactions.

The results in Fig. 5(d) were computed by partitioning the 100-bead chain into two halves: beads 1–50 had no reactive groups loaded, and beads 51–100 were equally loaded with a finite number of molecules. The chain was thus split into light and heavy segments, the former being akin to the portion that lies behind the reaction front. The kinetic energies of each bead were recorded over 2048 time steps for numerical convenience and averaged over 100 independent runs. No reactions were executed during this timeframe, since the object was to determine the coupling between beads of different masses at the interface. The power spectra in Fig. 5(d) correspond to two reactive group loads and have been plotted for a light bead (50) and three heavy beads (51, 52, and 60). In the cases of two and three reactive groups/bead, it is evident that the coupling between the light and heavy beads is conducive to the appearance of modes beyond the band-edge (i.e., $\omega > 0.57$) of the latter. The effect is most prominent for the heavy bead that is directly connected to the lighter one, and progressively decays further into the loaded portion of the chain. We postulate that the presence of these localized

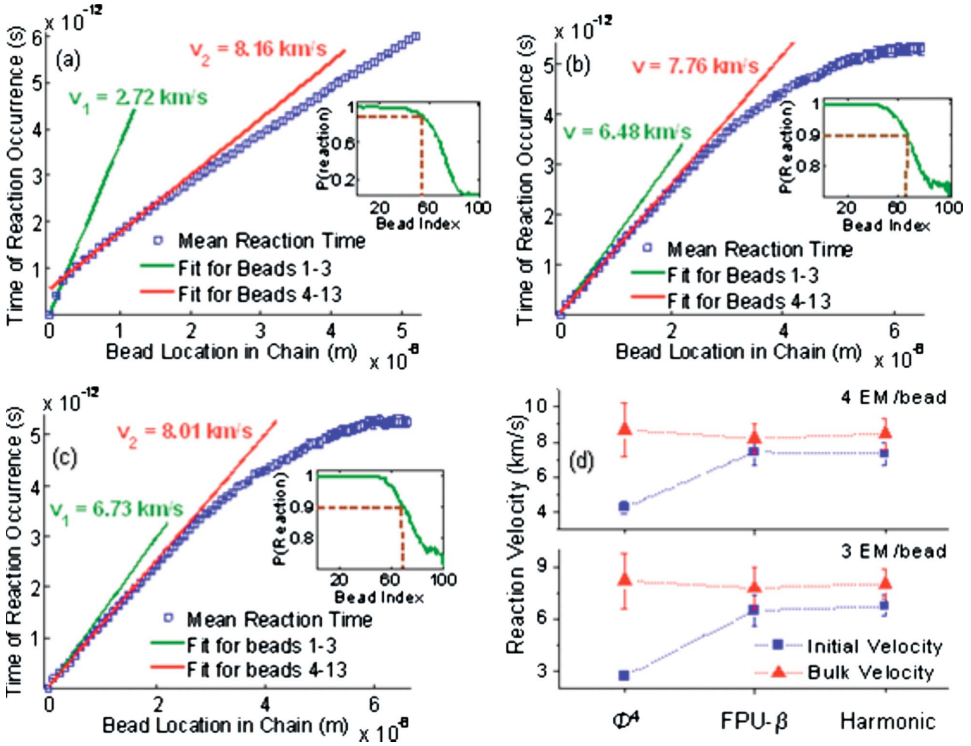

FIG. 6. (Color online) Comparison of reaction velocities for (a) φ^4, (b) FPU, and (c) harmonic lattices for 3 EM/bead (E_a =35 kcal/mol, α=0.7). Similar velocities are predicted for the FPU and harmonic cases, which are depicted in (d) for two different loadings. The insets in (a)–(c) show the probability cutoffs (0.90) that decided the number of viable reactions.

high-frequency modes in the heavier—or unreacted—beads causes them to react as soon as the preceding bead has reacted. A comparison of the two panels in Fig. 5(d) also shows that it is easier to induce higher modes in the case of lower EM loads (i.e., two versus three reactive groups/bead) simply because of the difference in bead mass, and hence, inertia.

C. Reaction Velocity Calculation

It is possible to extract the velocity of the reaction wave and the associated confidence intervals from these simulated data sets in the specific case of directional energy transfer. Reaction events with probabilities of occurrence below 0.90 were neglected during this calculation. Figures 6(a)–6(c) show the velocity calculations for three reactive groups/bead for the φ^4, FPU and harmonic lattices, respectively, with E_a=35 kcal/mol and α=0.7. The most probable reaction times at n beads can be easily fit with a straight line, the reciprocal slope of which is the velocity of the reaction wave. In each plot, we have separately fitted the reaction times at beads 1–3 and 4–13, respectively. This was necessitated by the presence of a distinct start-up zone for the φ^4 lattice [Fig. 6(a)], where the velocity computed from the first three beads (2.72 km/s) is a third of the bulk velocity computed from the next 10 beads (8.16 km/s). The FPU and harmonic lattices show a comparatively negligible difference in velocities between the two zones [Figs. 6(b) and 6(c)]. At a load of 3 EM/bead, the computed velocities are less than the speed of sound in the lattice ($\sim$14 km/s) and are therefore below the detonation limit.

The contrast between the initial and bulk velocities is clearly presented in Fig. 6(d) for two different loads of the energetic material. The φ^4 velocities predicted from beads 4–13 lie in the same range as the corresponding values for the other lattices within the 95% confidence intervals;[55,56] however, the reaction wave definitely undergoes an activation phase, which depends on the energetic load used. This conclusion is bolstered by the fact that the harmonic lattice displays similar behavior at a sparse loading of two groups/bead.[44] Furthermore, the difference between the two zones in the φ^4 lattice decreases as the loading is increased from four to seven reactive groups/bead.[44]

The predicted reaction times in the FPU and harmonic chains deviate considerably from the linear fit [Figs. 6(b) and 6(c)] as the distance from the ignition point increases. This observation points towards an increase in the wave velocity due to the energy injected into the lattice at each reacted node. The φ^4 chain, on the other hand, adheres to the linear reaction trajectory to a greater extent [Fig. 6(a)] even at higher energetic loads.[44] We have already seen that the variance in reaction times is less than the FPU and harmonic cases. The φ^4 lattice therefore offers a greater degree of control over the reaction trend although the overall conversion lags behind the other systems.

The reaction characteristics of the FPU-β and harmonic lattices are almost identical for the 3 EM/bead [Figs. 6(b) and 6(c)] and 4 EM/bead[44] scenarios. Previous work by Sarmiento *et al.*[8] has proved that pulse propagation in a hard anharmonic lattice occurs at speeds that exceed those in the harmonic variant. Since the energetic loads used thus far have been unable to distinguish between the two lattices, we increased the reaction enthalpy by a factor of 20 while keeping the load at two groups/bead. The corresponding velocity calculations are displayed in Figs. 7(a) and 7(b). Linear fits using the first 10 reaction times indeed show that the FPU-β has a marginally larger velocity (14.22 ± 0.28 km/s) than the harmonic chain (12.88 ± 0.57 km/s), thus showing that large deformations are required to distinguish between the two lattices.

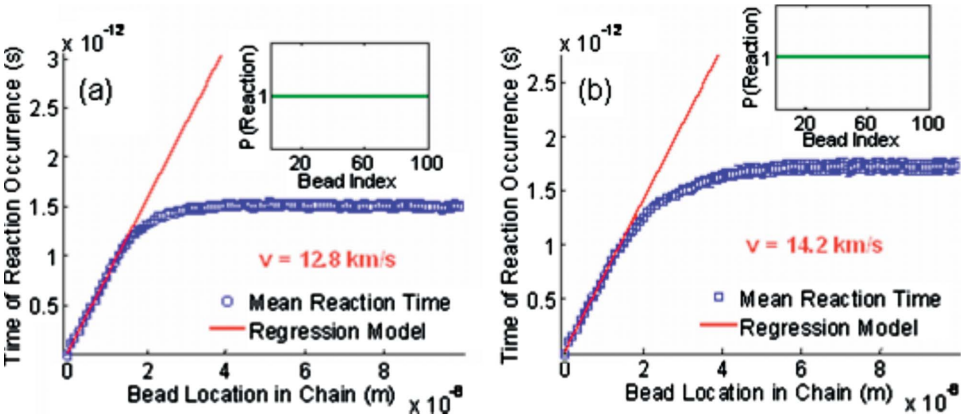

FIG. 7. (Color online) The reaction velocities for the (a) harmonic and (b) FPU lattices have been calculated for 2 EM/bead (E_a=35 kcal/mol, α=0.7) but with 20 times the reaction enthalpy as in the standard cases. The inset in each plot shows the variation in reaction probability with bead location.

D. Effect of Defects

Defects were introduced in the harmonic chain of oscillators by lowering the bond-stretch and bending force constants by a factor of 50 at select locations: 320 and 650 Å [Figs. 8(a) and 8(b)]. In a real nanotube, such a defect could represent a missing atom or a weaker carbon-carbon bond. The simulations were run for the three reactive groups/bead case and can therefore be compared with the conversion plot for the pristine chain in Fig. 3(a). The contour plot in Fig. 8(a) shows a distinct reduction in conversion with the presence of defects in comparison to Fig. 3(a). It is interesting to note that the average conversion at E_a=40 kcal/mol is around 70% even at α=1, whereas it was ~1 for the nondefective chains under similar circumstances. In addition, Fig. 8(b) shows that the very first defect in both cases drastically reduces the probability of reactions further down the length of the chain (inset). The reaction wave is disrupted by the defect at 320 Å; all the subsequent reactions shown in a lighter hue in the primary plot are comparatively rare events. The use of free boundary conditions at both ends of the chain results in more energetic beads at the extremes as compared to the central portion of the lattice,[44] and sometimes reactions at the end of the chain appear more likely than those in the center. Thus, defects may serve as a practical consideration making it difficult to experimentally realize these chain reactions in practice.

IV. CONCLUSIONS

We have a proposed a generic 1D nanostructure as a channel for directed energy transfer following chain reactions of energetic molecules attached to the lattice. Stability studies at four loadings of the EM showed that these assemblies are inherently unstable at activation energies below 25 kcal/mol. This sets a lower limit in the choice of EM during the design phase. A parametric study of chain reactions in both linear and nonlinear lattices showed that at loads of 3–4 EM/bead (E_a=35 kcal/mol, α=0.7), the FPU and harmonic lattices behaved similarly with reaction velocities ranging between 8–8.5 km/sec. The φ^4 lattice exhibited lower conversions along with the formation of a start-up zone where the reaction wave velocity was at least half of the bulk value at the aforementioned loads. Fourier analyses of the kinetic energy traces of the φ^4 lattice revealed that only high-frequency (i.e., high-energy) excitations led to viable wave propagation, which explains the prominence of the start-up zone at lower loadings of the energetic molecules. A similar study of the harmonic lattice KE indicates that the high-frequency modes contribute to reaction while the lower modes are concerned with energy propagation. Reaction velocities and associated confidence intervals have been computed for both pristine and defective harmonic chains. The latter show lower reactivities, as expected, due to poorer information transfer along the lattice—a direct consequence of the presence of defects.

ACKNOWLEDGMENTS

The authors would like to thank M. J. Buelher, L. V. Zhigilei, Y. Yingling, and G. Casati for clarifications regarding their respective models, W. H. Green for comments related to anharmonic potentials, and R. D. Braatz for material pertain-

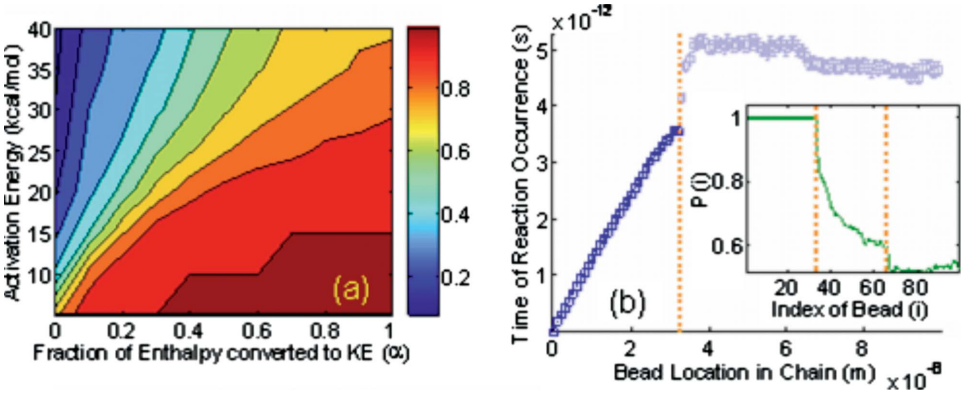

FIG. 8. (Color online) (a) Chemical conversion plot (3 EM/bead) for a harmonic chain with the introduction of two defects along its length. (b) The path of the reaction wave is impeded at the very first defect (orange dashed line), with the subsequent beads (light blue) having drastically reduced probabilities of reacting, as depicted in the inset.

ing to parameter estimation. We are also grateful to N. Chennamsetty, E. Santiso, A. Jayaraman, and S. Tejwani for their valuable inputs. Finally, we would like to acknowledge a grant from the Air Force Office of Scientific Research for carrying out this work.

[1] E. Fermi, J. Pasta, and S. Ulam, Report No. LA 1940, 1955 (unpublished).
[2] G. K. Straub, B. L. Holian, and R. G. Petschek, Phys. Rev. B **19**, 4049 (1979).
[3] G. Stoltz, Nonlinearity **18**, 1967 (2005).
[4] B. L. Holian and G. K. Straub, Phys. Rev. B **18**, 1593 (1978).
[5] J. N. Stember and G. S. Ezra, Chem. Phys. **337**, 11 (2007).
[6] R. Reigada, A. Sarmiento, and K. Lindenberg, Phys. Rev. E **64**, 066608 (2001).
[7] R. Reigada, A. Sarmiento, and K. Lindenberg, Physica A **305**, 467 (2002).
[8] A. Sarmiento, R. Reigada, A. H. Romero, and K. Lindenberg, Phys. Rev. E **60**, 5317 (1999).
[9] A. Rosas and K. Lindenberg, Phys. Rev. E **69**, 016615 (2004).
[10] M. S. Dresselhaus, G. Dresselhaus, and P. C. Eklund, *Science of Fullerenes and Carbon Nanotubes* (Academic Press, San Diego, 1996).
[11] R. Saito, G. Dresselhaus, and M. S. Dresselhaus, *Physical Properties of Carbon Nanotubes* (Imperial College Press, London, 1998).
[12] S. Berber, Y.-K. Kwon, and D. Tomanek, Phys. Rev. Lett. **84**, 4613 (2000).
[13] J. X. Cao, X. H. Yan, Y. Xiao, and J. W. Ding, Phys. Rev. B **69**, 073407 (2004).
[14] M. Grujicic, G. Cao, and W. N. Roy, J. Mater. Sci. **40**, 1943 (2005).
[15] N. Mingo and D. A. Broido, Nano Lett. **5**, 1221 (2005).
[16] M. A. Osman and D. Srivastava, Nanotechnology **12**, 21 (2001).
[17] E. Pop, D. Mann, Q. Wang, K. Goodson, and H. Dai, Nano Lett. **6**, 96 (2006).
[18] C. Yu, L. Shi, Z. Yao, D. Li, and A. Majumdar, Nano Lett. **5**, 1842 (2005).
[19] X. J. Hu, A. A. Padilla, J. Xu, T. S. Fisher, and K. Goodson, ASME J. Heat Transfer **128**, 1109 (2006).
[20] S. T. Huxtable, D. G. Cahill, S. Shenogin, L. Xue, R. Ozisik, P. W. Barone, M. L. Usrey, M. S. Strano, G. Siddons, M. Shim, and P. Keblinski, Nature Mater. **2**, 731 (2003).
[21] P. A. Childs and A. G. O' Neill, Physica E (Amsterdam) **19**, 153 (2003).
[22] G. F. Calvo and R. F. Alvarez-Estrada, Nanotechnology **15**, 1870 (2004).
[23] M. J. Buehler, F. F. Abraham, and H. Gao, Nature (London) **426**, 141 (2003).
[24] M. J. Buehler and H. Gao, Nature (London) **439**, 307 (2006).
[25] M. J. Buehler, J. Mater. Res. **21**, 2855 (2006).
[26] L. V. Zhigilei, C. Wei, and D. Srivastava, Phys. Rev. B **71**, 165417 (2005).
[27] L. V. Zhigilei, P. B. Kodali, and B. J. Garrison, J. Phys. Chem. B **101**, 2028 (1997).
[28] Y. Yingling and B. J. Garrison, J. Phys. Chem. B **108**, 1815 (2004).
[29] M. Prasad, P. F. Conforti, and B. J. Garrison, J. Chem. Phys. **127**, 084705 (2007).
[30] A. M. Kosevich, *The Crystal Lattice: Phonons, Solitons, Dislocations, Superlattices* (Wiley, Weinheim, 2005).
[31] A. C. Newell, *Solitons in Mathematics and Physics* (Society for Industrial and Applied Mathematics, Philadelphia, 1985).
[32] J. L. Marin, S. Aubry, and L. M. Floria, Physica D **113**, 283 (1998).
[33] G. P. Tsironis and S. Aubry, Phys. Rev. Lett. **77**, 5225 (1996).
[34] R. Reigada, A. H. Romero, A. Sarmiento, and K. Lindenberg, J. Chem. Phys. **111**, 1373 (1999).
[35] G. P. Tsironis, A. R. Bishop, A. V. Savin, and A. V. Zolotaryuk, Phys. Rev. E **60**, 6610 (1999).
[36] R. Reigada, A. Sarmiento, A. H. Romero, J. M. Sancho, and K. Lindenberg, J. Chem. Phys. **112**, 10615 (2000).
[37] J. T. Abrahamson, N. Nair, and M. S. Strano, Nanotechnology **19**, 195701 (2008).
[38] W.-J. Kim, N. Nair, C. Y. Lee, and M. S. Strano, J. Phys. Chem. C **112**, 7326 (2008).
[39] N. Nair, W.-J. Kim, M. L. Usrey, and M. S. Strano, J. Am. Chem. Soc. **129**, 3946 (2007).
[40] M. S. Strano, C. A. Dyke, M. L. Usrey, P. W. Barone, M. J. Allen, H. W. Shan, C. Kittrell, R. H. Hauge, J. M. Tour, and R. E. Smalley, Science **301**(5639), 1519 (2003).
[41] M. L. Usrey, E. S. Lippmann, and M. S. Strano, J. Am. Chem. Soc. **127**, 16129 (2005).
[42] D. T. Gillespie, J. Comput. Phys. **22**, 403 (1976).
[43] D. T. Gillespie, J. Phys. Chem. **81**, 2340 (1977).
[44] See EPAPS Document No. E-PRBMDO-80-056937 for calculations for higher loads, thermal counductivities and the effect of energetic loading on the φ^4 phonon spectrum. For more information on EPAPS, see http://www.aip.org/pubservs/epaps.html.
[45] H. Muthurajan, R. Sivabalan, M. B. Talawar, M. Anniyappan, and S. Venugopalan, J. Hazard. Mater. **133**, 30 (2006).
[47] B. Hu, B. Li, and H. Zhao, Phys. Rev. E **61**, 3828 (2000).
[48] S. Lepri, R. Livi, and A. Politi, Phys. Rev. Lett. **78**, 1896 (1997).
[49] S. Lepri, R. Livi, and A. Politi, Phys. Rep. **377**, 1 (2003).
[50] S. Lepri, R. Livi, and A. Politi, Phys. Rev. E **68**, 067102 (2003).
[51] S. R. Calvo and P. B. Balbuena, Surf. Sci. **581**, 213 (2005).
[52] M. Hu, P. Keblinski, and B. Li, Appl. Phys. Lett. **92**, 211908 (2008).
[53] B. Li, L. Wang, and G. Casati, Phys. Rev. Lett. **93**, 184301 (2004).
[54] J. M. Bowman, X. Zhang, and A. Brown, J. Chem. Phys. **119**, 646 (2003).
[55] R. Gunawan, M. Y. L. Jung, E. G. Seebauer, and R. D. Braatz, AIChE J. **49**, 2114 (2003).
[56] J. V. Beck and K. J. Arnold, *Parameter Estimation in Engineering and Science* (Wiley, New York, 1977).